FEBS Letters 585 (2011) 2568–2574

journal homepage: www.FEBSLetters.org

Mutant ubiquitin (UBB^{+1}) associated with neurodegenerative disorders is hydrolyzed by ubiquitin C-terminal hydrolase L3 (UCH-L3)

Frank J.A. Dennissen [a], Natalia Kholod [a], Denise J.H.P. Hermes [a], Nadja Kemmerling [a], Harry W.M. Steinbusch [a], Nico P. Dantuma [b], Fred W. van Leeuwen [a,*]

[a] Department of Neuroscience, Faculty of Health Medicine and Life Sciences, Maastricht University, Universiteitssingel 50, P.O. Box 616, 6200 MD Maastricht, The Netherlands
[b] Department of Cell and Molecular Biology (CMB), Karolinska Institutet, von Eulers väg 3, P.O. Box 285, S-17177 Stockholm, Sweden

ARTICLE INFO

Article history:
Received 29 March 2011
Revised 28 June 2011
Accepted 30 June 2011
Available online 6 July 2011

Edited by Noboru Mizushima

Keywords:
UBB^{+1}
Ubiquitin C-terminal hydrolase L3
Yeast ubiquitin hydrolase 1
Alzheimer's disease

ABSTRACT

Mutant ubiquitin (UBB^{+1}) accumulates in the hallmarks of tauopathies and polyglutamine diseases. We show that the deubiquitinating enzyme YUH1 of *Saccharomyces cerevisiae* and its mouse and human ortholog UCH-L3 are able to hydrolyze the C-terminal extension of UBB^{+1}. This yields another dysfunctional ubiquitin molecule (UB^{G76Y}) with biochemical properties similar to full length UBB^{+1}. UBB^{+1} may be detected in post-mortem tissue due to impaired C-terminal truncation of UBB^{+1}. Although the level of UCH-L3 protein in several neurodegenerative diseases is unchanged, we show that *in vitro* oxidation of recombinant UCH-L3 impairs its deubiquitinating activity. We postulate that impaired UCH-L3 function may contribute to the accumulation of full length UBB^{+1} in various pathologies.

1. Introduction

Ubiquitin is essential for cellular homeostasis. Polyubiquitin chains are conjugated to proteins designated for proteasomal degradation by an ubiquitin activating enzyme (E1), a ubiquitin conjugating enzyme (E2), and a ubiquitin ligase (E3) [1]. For polyubiquitination, the C-terminal glycine of one ubiquitin molecule is conjugated to one of the internal lysines of another ubiquitin molecule [1].

Ubiquitination is counterbalanced in humans by nearly 100 deubiquitinating enzymes (DUBs) which are essential for (re)generation of ubiquitin [2] and controlling epigenetic mechanisms by deubiquitinating histones [2,3]. DUBs can, for example, protect proteins from degradation by deubiquitination [4] but also assist in proteasomal degradation through deubiquitination of substrates after binding to the proteasome [5]. One subfamily of DUBs is the group of ubiquitin C-terminal hydrolases (UCHs). UCHs are able to hydrolyze ubiquitin precursor proteins and to remove small adducts from ubiquitin in vitro [6]. At least one enzyme belonging to this family, UCH-L1, is genetically linked to neurodegenerative disorders [7,8].

In many neurodegenerative disorders aberrant proteins aggregate and accumulate in inclusions which often contain ubiquitin [9,10]. Moreover, impaired proteasome function, mutated ubiquitin hydrolases and specific ubiquitin ligases have been implicated in neurodegenerative disorders [7,11–13]. This suggests that dysfunction of the ubiquitin–proteasome system (UPS) may play a role in these diseases.

In Alzheimer's disease (AD) and other tauopathies as well as polyglutaminopathies, a mutant ubiquitin (UBB^{+1}), which is encoded by an erroneously transcript [14], colocalizes with the hallmarks (e.g., neurofibrillary tangles and neuritic plaques) associated with these pathologies [14,15] while it was undetectable in brains of young controls and in synucleinopathies. UBB^{+1} mRNA was found in all brains tested [16] which suggests that healthy individuals are able to process UBB^{+1} while UBB^{+1} accumulates in affected brains. UBB^{+1} mRNA codes for a ubiquitin molecule with a C-terminal glycine to tyrosine substitution and an addition of 19 amino acids. Consequently, UBB^{+1} cannot be used for (poly)ubiquitination. UBB^{+1} impairs the UPS when ubiquitinated and ubiquitinated UBB^{+1} is refractory to disassembly by DUBs [17–19].

Although UBB^{+1} is targeted for proteasomal degradation [16], recent advances indicate that UBB^{+1} does not meet the prerequisites for efficient proteasomal degradation. Recent studies revealed that the C-terminal extension of UBB^{+1} is too short for efficient proteasomal degradation [20,21]. In the present study, we show that the UCH-L3 is able to cleave the C-terminus of UBB^{+1}. In addition, oxidation of UCH-L3 impairs its hydrolysis activity. We therefore propose that accumulation of UBB^{+1} may, in part, be due to

* Corresponding author.
E-mail addresses: f.dennissen@maastrichtuniversity.nl (F.J.A. Dennissen), F.vanLeeuwen@maastrichtuniversity.nl (F.W. van Leeuwen).

0014-5793/$36.00 Crown Copyright © 2011 Published by Elsevier B.V. on behalf of Federation of European Biochemical society. All rights reserved.
doi:10.1016/j.febslet.2011.06.037

inefficient hydrolysis of the C-terminus of UBB^{+1}. Our in vitro data suggest that impaired truncation is caused by inactivation of UCH-L3 in the oxidative environment that has been shown to be associated with various neurodegenerative disorders [22].

2. Materials and methods

2.1. Plasmids

The generation of plasmids for pCMV-$^{myc}UBB^{+1}$, pCMV-$^{myc}UB^{G76V}$, pCMV-$^{myc}UBB^{+1}$ K0 and pYES2-$^{myc}UBB^{+1}$ was described previously [21]. For cloning of the UCHs, mRNA from HEK293 cells or hippocampus from human and mouse was isolated with standard Trizol–chloroform extraction methods after which cDNA was generated using the first strand synthesis kit (Fermentas). The cDNA for the UCHs was PCR amplified and cloned into a pEF5-HA vector [23] (Supplementary Table 1). Human UCH-L3 was subcloned into pET28a according to a standard protocol. Cloned DNA fragments were sequenced (GATC-Biotech) to control for mutations. For transfection of cells all plasmids were amplified and isolated with maxiprep kit (Qiagen).

2.2. Antibodies

All the antibodies and antibody dilutions can be found in Supplementary Table 2.

2.3. Yeast strains, growth and transformation of the yeast miniscreen

The miniscreen was generated by selecting 175 deletion strains (Supplementary Fig. 1 and Supplementary Table 3) from the genome wide deletion collection (BY4741 MATa his3Δ1 leu2Δ0 met15Δ0 ura3Δ0 background, kind gift from Dr. F. van Leeuwen, NKI, Amsterdam) on YPD-agar (1% bacto-yeast extract, 2% bacto-peptone, 2% dextrose, 2% agar) plates in a 96-well format. Selection criteria were that the gene was involved in protein quality control and/or protein/peptide degradation (Table 1).

Yeast transformation was performed according to a modified version of a method described for microtiter plate transformation using the LiAc/SS carrier DNA/PEG [24] (Supplementary Fig. 1).

All transformed yeast strains were grown to a density with an $A_{600} \approx 1.0$, collected and dissolved in 17% trichloroacetic acid (TCA) to isolate their proteins.

2.4. SDS–PAGE and immunoblotting

The precipitated protein pellets from yeast as well as the pelleted mammalian cells were dissolved in 200 μl of loading buffer containing 130 mM Tris–HCl, pH 8.0, 10% (v/v) Glycerol, 2.3% (w/v) SDS, 1% DTT and 0.1% bromephenolblue and resolved by SDS–PAGE on 12% Bis-Tris Gels (NuPAGE® Novex, Invitrogen) or 16% Tris-Tricine gel, transferred to nitrocellulose membranes (pore size 0.2 μm, Invitrogen) and immunostained according to standard protocol [25]. Proteins were visualized by an enhanced chemiluminescence (ECL™, Amersham) or with the Odyssey® scanner (LI-COR). When using a HRP-conjugated labeled secondary antibody, loading control (β-actin) was stained consecutively after detection of the protein of interest. For the IRDye labeled secondary antibodies, two differently labeled antibodies were used which could be detected independently by multi-fluorescence scanning of the Odyssey® system (LI-COR). The UCH-L3 protein of AD and control patients were immunoblotted according to the standard Odyssey® manufacturing protocol and double stained for UCH-L3 and GAPDH for loading control.

Table 1
The number of genes per category used for the miniscreen.

Categories	Number of genes
Chaperones and protein transport	19
UPS	62
Autophagy	4
Protein sorting	9
Neddylation and sumoylation	8
Deubiquitinases	16
Peptidases/metalloproteases	55
Miscellaneous	2

2.5. Mammalian cell culture and transfection

HEK293 and HeLa cells stably transfected with a reporter for the ubiquitin fusion degradation (UFD) pathway (HeLa UB^{G76V}-GFP) [26] were cultured in Dulbecco's modified Eagle's medium (Gibco) supplemented with 10% of fetal calf serum (BODINCO), 50 units/ml of penicillin (Gibco) and 50 units/ml of streptomycin (Gibco). For transfections, 2 μg of plasmid DNA and 6 μg of Polyethylenamine "Max" (Polysciences) were mixed in 50 μl PBS. Solutions were incubated at room temperature for 15 min and subsequently added to cells in 1 ml of serum and antibiotic free Dulbecco's modified Eagle's medium (DMEM) (Gibco). The culture medium was changed 4–5 h after transfection to fresh-serum-supplemented DMEM.

2.6. Mass spectrometry (MS) of truncated UBB^{+1}

HEK293 cells were transiently transfected with pEF5HA-UCH-L3; 24 h later cells were harvested and lysed in lysis buffer containing 50 mM Tris–HCl (pH 7.6), 50 mM NaCl and 5 mM DTT. Ten micrograms of recombinant $^{HIS}UBB^{+1}$ was added to 50 μl of the lysate (50 mg/ml total protein) and incubated overnight at 37 °C. $^{HIS}UBB^{+1}$ and truncated $^{HIS}UBB^{+1}$ were purified by using TALON™ Immobilized Metal Affinity Chromatography (IMAC) Resin (BD-Biosciences) according to the manufacturer's recommendation. Samples were resolved by SDS–PAGE gel electrophoresis after which the bands corresponding to full-length and truncated UBB^{+1} were cut and digested according to the method of Shevchenko et al. [27]. The mass spectrometric (MS) analysis was carried out using a MALDI-TOF/TOF instrument (4800 Proteomics Analyzer, Applied Biosystems) with reflector positive ion mode. For MS analysis, 800–3000 m/z mass range was used with 1250 shots per spectrum. A maximum of 20 precursors per spot with minimum signal/noise ratio of 50 were selected for data-dependent MS/MS analysis. A 1-kV collision energy was used for CID, and 2500 acquisitions were accumulated for each MS/MS spectrum.

2.7. The effect of UBB^{+1} truncation by UCH-L3 on UFD-pathway inhibition

HeLa UB^{G76V}-GFP reporter cells were seeded on coverslips. The cells were transiently transfected with $^{myc}UBB^{+1}$ or $^{myc}UB^{+1}$ 24 h post-seeding. The cells were fixed 24 h post-transfection and stained for the myc tag. The slides were analyzed using a IX81 motorized inverted microscope (Olympus).

2.8. Turnover of full length UBB^{+1}, truncated UBB^{+1} (UB^{G76Y}) and UB^{G76V} + 25 in vitro

HEK293 cells were transiently transfected with $^{myc}UBB^{+1}$, $^{myc}UBB^{G76Y}$ or UB^{G76V} + 25. Cells were transfected with UB^{G76V} + 25 for turnover control since this extended dysfunctional ubiquitin is degraded by the proteasome [21]. Turnover was determined 24 h

post-transfection by adding cycloheximide to the medium with a final concentration 50 μg/ml. Cells were harvested for Western blot analysis at 0, 1, 2, 4, 6 and 8 h after blocking translation. Cells were also treated with proteasome inhibitor Bortezomib (10 nM) to determine the effect of inhibition of the proteasome on steady state levels of the UB^x species. Membranes were probed with anti-myc and anti-GAPDH antibodies for loading control.

2.9. Production of recombinant ^{HIS}UCH-L3, $^{HIS}UBB^{+1}$ and generation of the +1 peptide

Recombinant ^{HIS}UCH-L3 and $^{HIS}UBB^{+1}$ were generated according to a standard protocol. Rosetta™ bacteria were transformed with pET28a-^{HIS}UCH-L3 or pET28a-$^{HIS}UBB^{+1}$ and grown overnight in selective medium (25 μg/ml of kanamycin) at 37 °C. Overnight cultures were diluted into 5 ml selective medium to OD_{600} = 0.1 and incubated at 37 °C. After growing to OD_{600} = 0.8 isopropyl beta-D-thiogalactoside (IPTG) was added to a final concentration of 1 mM. Bacteria were incubated at 37 °C with IPTG for 4 h, pelleted and frozen until further processing. ^{HIS}UCH-L3 and $^{HIS}UBB^{+1}$ were purified using BD TALON™ Metal Affinity Resin according to the manufacturer's protocol. One microgram of ^{HIS}UCH-L3 and 5 μg of $^{HIS}UBB^{+1}$ were mixed in 50 μl of lysis buffer (see Section 2.6) and incubated overnight at 37 °C. Loading buffer was added and proteins were resolved by SDS–PAGE (see Section 2.4). $^{HIS}UBB^{+1}$ was stained with Coomassie or immunoblotted with anti-HIS and UBI-3 antibodies.

2.10. The effect of oxidation on UCH-L3 activity

Recombinant ^{HIS}UCH-L3 was incubated in 25 mM HEPES buffer (pH 7.2) or in 25 mM HEPES buffer (pH 7.2) containing 25 mM ascorbate and 100 μM $FeCl_3$ for 5 h at 37 °C. Analysis of normal, oxidized or inhibited UCH-L3 activity was done by co-incubating with $^{HIS}UBB^{+1}$ as has been described (see Section 2.9). UCH-L3 was inhibited by adding UCH-L3 inhibitor (4,5,6,7-Tetrachloroindan-1,3-dione, Calbiochem) to the mix at a final concentration of 10 μM.

2.11. UCH-L3 quantification in post-mortem tissue from AD, PD, HD and control patients

Fresh frozen hippocampus tissue of AD and control brains, fresh frozen cingulate gyrus (BA24) of PD and control brains and fresh frozen prefrontal cortex of HD and control brains (Supplementary Table 4) were homogenized in lysis buffer containing 50 mM Tris–HCl (pH 7.6) and 50 mM NaCl at 4 °C. Total protein concentration was determined with the Bio-Rad protein assay. After SDS–PAGE and transfer, the membrane was immunoblotted with anti-UCH-L3 and anti-GAPDH antibodies. Quantification was performed with the LI-COR analysis software after multi-fluorescence scanning of the membrane [28].

2.12. Statistical analysis

The difference in UCH-L3 quantity has been tested with a 2-sided distribution free Mann–Whitney test (accepted level of significance $P < 0.05$).

3. Results and discussion

3.1. Loss of YUH1 gene abolishes the C-terminal truncation of UBB^{+1}

To study post-translational processing of myc-tagged UBB^{+1} ($^{myc}UBB^{+1}$) *in vivo*, *Saccharomyces cerevisiae* (baker's yeast) was used as a model organism. A selection of 175 yeast deletion strains from a genome-wide deletion library was made to assemble the miniscreen (Supplementary Table 1).

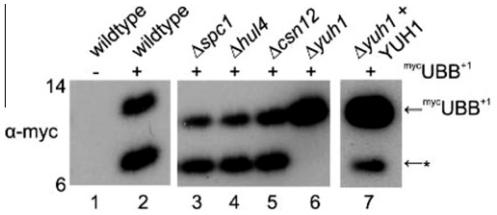

Fig. 1. Yeast ubiquitin hydrolase 1 (YUH1) is responsible for C-terminal truncation of human UBB^{+1} in *S. cerevisiae*. Western blot of a section of the miniscreen. The Δ*yuh1* deletion strain cannot truncate $^{myc}UBB^{+1}$ (lane 6). Ectopic expression of recombinant YUH1 restores truncation of $^{myc}UBB^{+1}$ in the Δ*yuh1* strain (lane 7).

In the yeast strains, we detected in addition to UBB^{+1} a truncated product of UBB^{+1} (size ≈ 11 kDa) that corresponds to the size of myc-tagged ubiquitin (Fig. 1B, lanes 2–6). We observed the truncated product in all tested deletion strains except for the Δ*yuh1* strain which is lacking the yeast ubiquitin hydrolase 1 gene (lane 6). Processing of $^{myc}UBB^{+1}$ could be rescued in the Δ*yuh1* strain by ectopic expression of YUH1 confirming that this enzyme is required for processing of $^{myc}UBB^{+1}$ (lane 7).

3.2. Human and mouse UCH-L3 are able to hydrolyze the UBB^{+1} C-terminus and generate truncated UBB^{+1} (UB^{G76Y})

YUH1 is member of the ubiquitin carboxy-terminal hydrolase (UCH) family. In humans this family consist of: UCH-L1, UCH-L3, UCH-L5 and BAP-1 of which UCH-L3 shows the highest homology with YUH1 (Table 2). Mice express UCH-L4, a close homolog of UCH-L3, in addition to the human enzymes (Table 3). We cloned cDNAs coding for UCH-L1, UCH-L3 and UCH-L5 of both mouse and human and UCH-L4 of mouse into an expression vector. We also cloned the CRA_f isoform of UCH-L3 from human cDNA, a naturally occurring UCH-L3 isoform missing amino acids 15–18 (VTNQ). These amino acids are part of a putative substrate-binding site of UCH-L3 and presumably the CRA_f isoform has lost its affinity for ubiquitin [29]. HEK293 cells were transiently co-transfected with UBB^{+1} and the respective peptidases (Fig. 2A). Cleavage of UBB^{+1} is strikingly increased when co-transfected with UCH-L3 (Fig. 2A, lanes 3 and 7). Transfection with the CRA_f isoform of UCH-L3 (lane 4), UCH-L4 (lane 8), UCH-L1 (lanes 2 and 6) or UCH-L5 (lanes 5 and 9) did not result in an increase in truncated

Table 2
Homology between *S. cerevisiae* YUH1 and human UCH family members.

	Score	E-value	Positives (%)	Identity (%)
UCH-L3	286	3.0E−25	51	32
UCH-L1	206	6.0E−16	51	30
UCH-L5	134	1.0E−7	43	27
BAP1	88	3.1E−2	41	25

Table 3
Homology between mouse and human UCH family members.

	Score	E-value	Positives (%)	Identity (%)
UCH-L1	1119	1.0E−122	99	95
UCH-L3	1188	1.0E−130	100	98
UCH-L4[a]	1145	1.0E−125	97	94
UCH-L5	1653	0.0	99	96
BAP1	3500	0.0	95	93

[a] UCH-L4 is aligned with human UCH-L3.

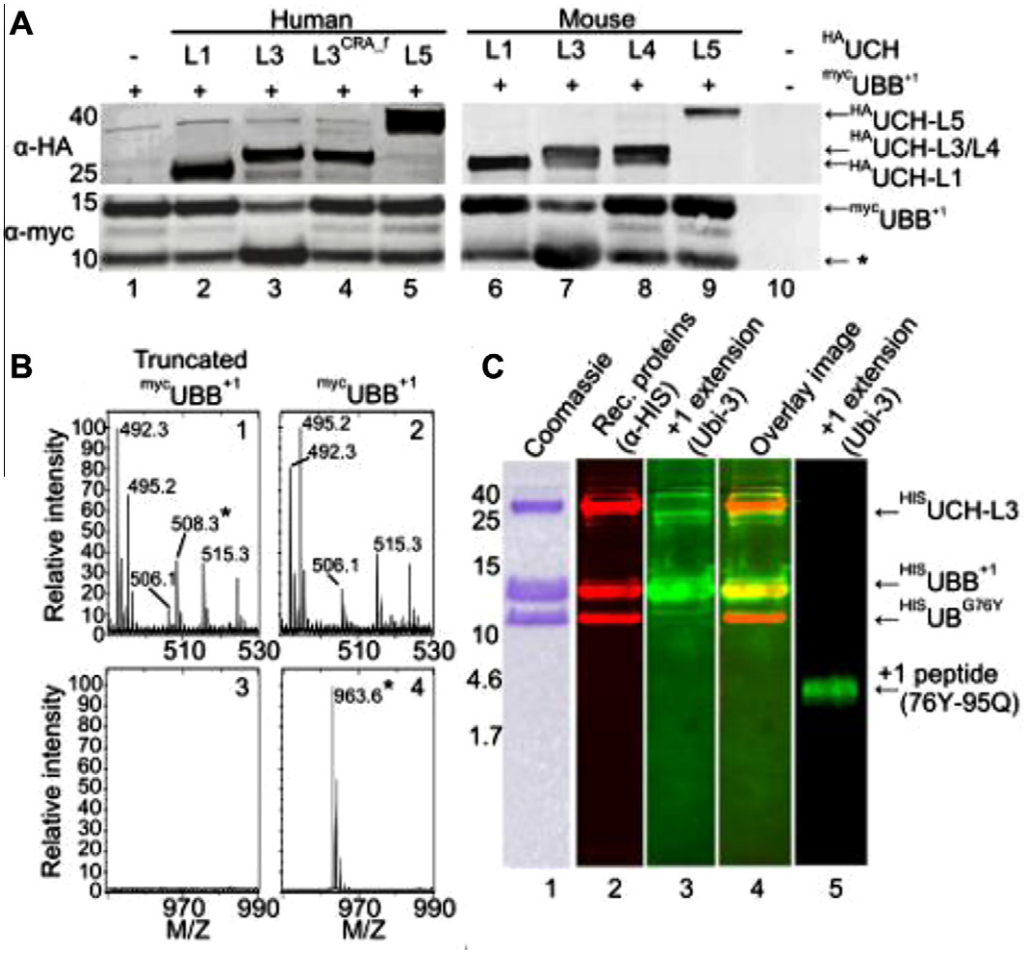

Fig. 2. Human and mouse UCH-L3 are able to truncate human UBB^{+1} yielding UB^{G76Y} but no intact C-terminal peptide. (A) UBB^{+1} is a substrate for UCH-L3 from human and mouse. The asterisk marks the truncated UBB^{+1} product. (B) Identification of the hydrolysis site in UBB^{+1} by UCH-L3. Two peptides are unique (asterisks) and correspond to LRGY (panel 1, 508.3*) and LRGYADLR (panel 4, 963.6*). (C) Truncation of recombinant $^{HIS}UBB^{+1}$ by recombinant ^{HIS}UCH-L3 (lane 1). Immunostaining with anti-HIS-tag antibodies in red (lane 2) and immunostaining using antibodies raised against the C-terminal extension of UBB^{+1} (UBI-3) in green (lane 3). Artificial peptide corresponding to the C-terminal extension of UBB^{+1} is shown as a positive control (lane 5).

UBB^{+1} indicating that they do not contribute to UBB^{+1} truncation. The truncated species observed in the UBB^{+1} single transfection control is due to the endogenous C-terminal hydrolyze activity in HEK293 cells. To determine the hydrolysis site in UBB^{+1} by UCH-L3, we incubated recombinant $^{HIS}UBB^{+1}$ with an extract of HEK293 cells transfected with human ^{HA}UCH-L3. Resolving proteins on high resolution SDS–PAGE and subsequent Coomassie staining yielded two distinct bands corresponding to UBB^{+1} and truncated UBB^{+1}. The mass spectrometry data revealed that one peptide was unique to truncated ubiquitin (LRGY, Fig. 2B, top panels) while full length UBB^{+1} yielded a different peptide (LRGYADLR, Fig. 2B, lower panels) This finding reveals that the truncated species was indeed C-terminally truncated UBB^{+1} with the final amino acid being tyrosine 76 (Y76). Truncation of UBB^{+1} prevents detection by antibodies raised against its C-terminus. Both truncated and full length UBB^{+1} could be detected by Coomassie staining (Fig. 2C, lane 1) and by using antibodies against the N-terminal myc-tag (Fig. 2C, lane 2). Accordingly, the UBI-3 antibody, which specifically recognizes the +1 extension, reacted with the full length UBB^{+1} while we were unable to detect UB^{G76Y} (Fig. 2C, lane 3). The cleaved +1 peptide could not be detected by Coomassie staining or by using the UBI-3 antibodies (Fig. 2C, lanes 1 and 3). Previously, it was shown that the UCH of *Drosophila melanogaster* (UCH-D) could not cleave the C-terminal extension of UBB^{+1} [18]. It was proposed that any residue larger than glycine at position 76 would result in a steric clash with Asn88 of YUH1 [30]. Consequently, it was concluded that UBB^{+1} was unsusceptible to cleavage by any UCH enzyme and that the C-terminal double glycine (G75 and G76) was essential for hydrolysis. Indeed, all known substrates (NEDD8 and ubiquitin) of UCH-L3 possess a C-terminal double glycine. In the present paper we show that, contradictory to the literature, UCH-L3 and YUH1 are able to cleave the C-terminal extension of UBB^{+1} despite the fact that the C-terminal glycine is substituted with a tyrosine.

3.3. Full length and truncated UBB^{+1} are slowly degraded in vitro and inhibit the ubiquitin fusion degradation (UFD)-pathway

UPS function can be studied by expressing a ubiquitin-GFP fusion protein. The UB^{G76V}-GFP reporter substrate is degraded by the proteasome by a well-mapped functional cascade of proteins (UFD-pathway). Impairment of one or more proteins involved in this cascade, including the proteasome, causes accumulation of UB^{G76V}-GFP. To determine the effect of truncated UBB^{+1} (UB^{G76Y}) on the UFD-pathway reporter, UB^{G76Y} was transiently transfected in HeLa UB^{G76V}-GFP cells. Normally, this reporter is rapidly degraded resulting in low steady state levels (Fig. 3A). UBB^{+1} induced UFD-impairment (Fig. 3A and B) as shown previously [17]. Impairment also occurred by introduction of truncated UBB^{+1} (UB^{G76Y}, Fig. 3A and B). UBB^{+1} has been reported to be too short to be

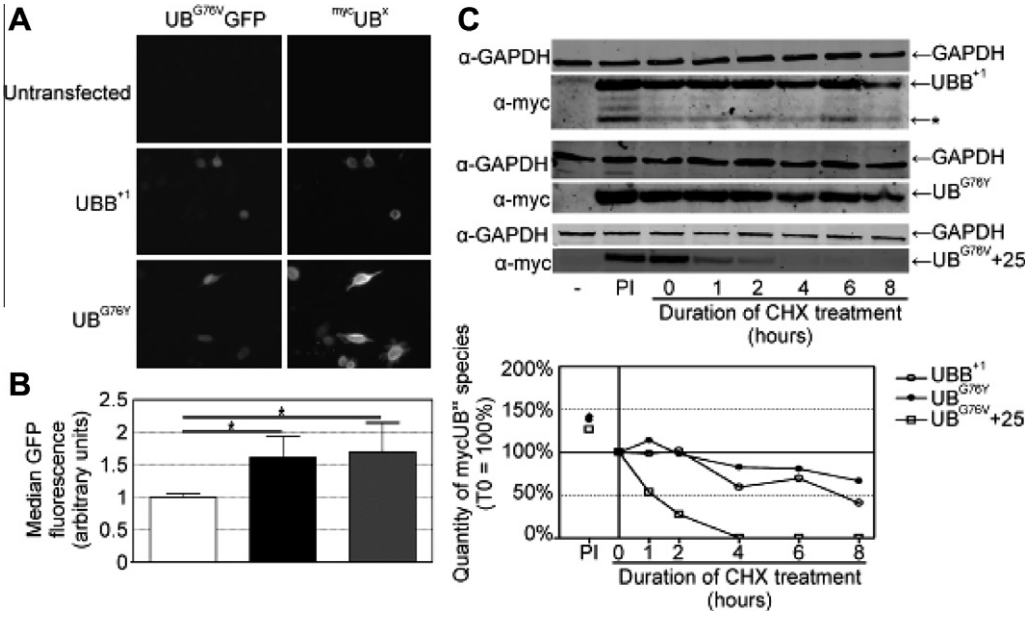

Fig. 3. UB^{X} species in UB^{G76V}-GFP reporter cells show impairment of the UFD-pathway for dysfunctional ubiquitin. UBB^{+1} and UB^{G76Y} impair the UFD-pathway (panels A and B). Full length UBB^{+1} and UB^{G76Y} are equally slowly degraded in vitro while UB^{G76V} + 25 is undetectable after 2 h (panel C). Bortezomib increases steady state levels of UB^{X} species to 125–150% of normal levels. The asterisk marks the truncated UBB^{+1} species.

degraded by the proteasome [21]. A dysfunctional ubiquitin lengthened by an additional 25 amino acids (UB^{G76V}+25) is, however, efficiently degraded by the proteasome. To determine the degradation rate of UB^{G76Y} compared to UBB^{+1} and UB^{G76V}+25 turnover was assessed by cycloheximide chase analysis and Western blotting. $^{myc}UB^{G76Y}$ and UBB^{+1} are slowly degraded in HEK293 cells (Fig. 3C). The half life of these species is approximately 8 h, whereas UB^{G76V}+25 has a half life of approximately 30 min. Truncation of UBB^{+1} generates a new species which could have different properties compared to full length UBB^{+1}. However, both

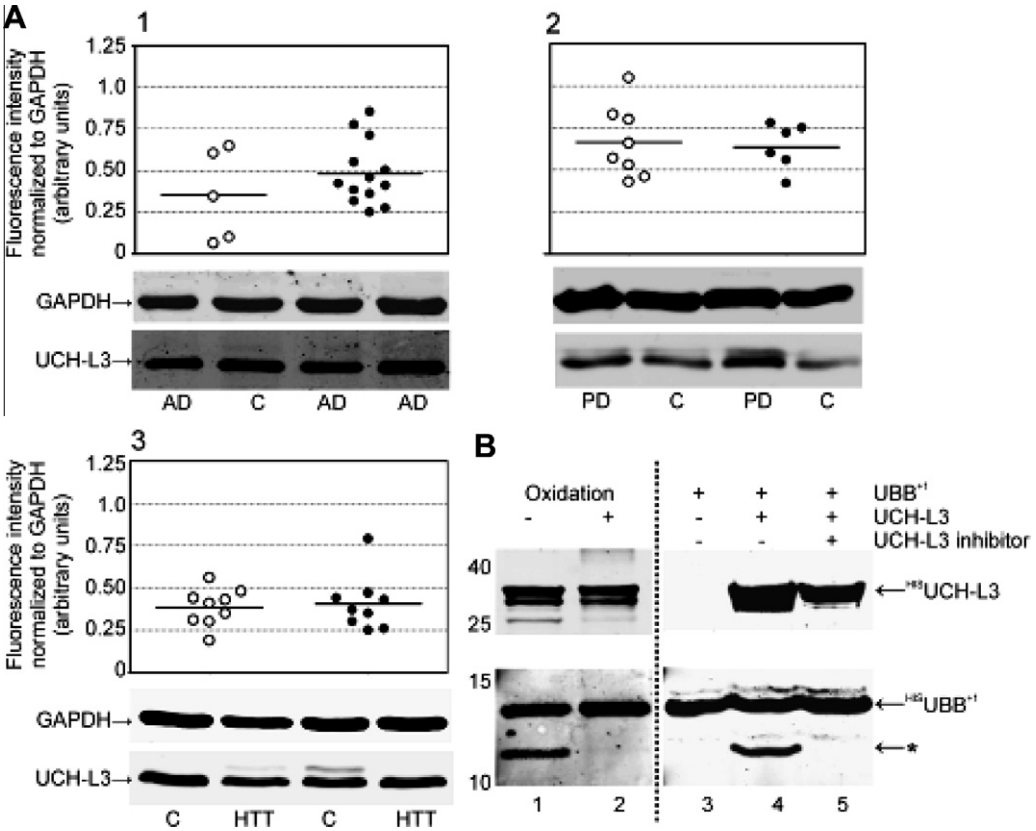

Fig. 4. Levels of UCH-L3 in AD, PD and HD and the effect of oxidation of UCH-L3 on hydrolysis activity. (A) UCH-L3 levels are unchanged in: AD (panel 1), PD (panel 2) and HD (panel 3) compared to controls. (B) In vitro oxidized UCH-L3 is unable to hydrolyze the C-terminal extension of UBB^{+1} and the catalytic activity of UCH-L3 is essential for truncation. Truncated species are marked with ⁎.

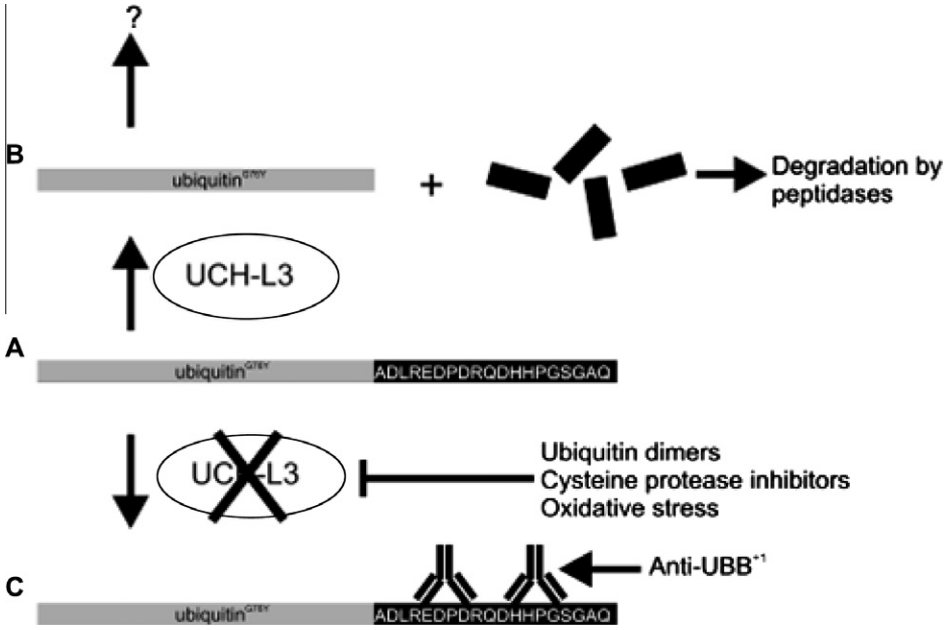

Fig. 5. Hypothesis to explain the selective detection of UBB^{+1} in post-mortem tissue of neurodegenerative disorders. (A) UBB^{+1} is generated at a slow rate in humans. (B) Normally the C-terminal extension of UBB^{+1} is hydrolyzed by a C-terminal hydrolase (e.g., UCH-L3). (C) With impaired hydrolase activity there is accumulation of UBB^{+1} giving rise to UBB^{+1} immunoreactivity in post-mortem tissue.

species are poorly degraded and UB^{G76Y} impairs the UFD pathway similar to UBB^{+1}. Truncated and full length UBB^{+1} both impair the UFD-pathway and show equally slow turnover rates. Therefore, it is not to be expected that (impaired) truncation contributes to neurodegeneration.

3.4. Levels of UCH-L3 are unchanged in neurodegenerative disorders but UCH-L3 activity is blocked when oxidized

To determine if UCH-L3 levels are changed in neurodegenerative disorders related to presence of UBB^{+1}, we quantified UCH-L3 by Western blotting (Fig. 4A). No statistical significant difference was found between AD patients, PD patients or HD patients (closed bullets) and their respective controls (open bullets).

Oxidative stress is a known feature of neurodegenerative disorders. Cysteine proteases such as UCH-L3 have been known to be vulnerable to oxidation [8]. Indeed, truncation of $^{HIS}UBB^{+1}$ by ^{HIS}UCH-L3 (Fig. 4B, lane 1) is blocked when ^{HIS}UCH-L3 is oxidized (Fig. 4B, lanes 1 and 2). Similar results were obtained by inhibiting the catalytic activity of UCH-L3 by a selective UCH-L3 inhibitor (Fig. 4B, lanes 4 and 5). It has been reported that UCH-L1 is upregulated in AD while at the same time it is damaged by oxidative modification reducing net enzyme activity to 30% of the normal level [8]. Our in vitro data suggest that its closely related isozyme UCH-L3 may face a similar fate when exposed to oxidative stress resulting in accumulation of full length UBB^{+1} (Fig. 5). We attempted to determine the UCH-L3 enzyme activity in protein lysates of human hippocampi (AD and control tissue). Using human post-mortem tissue lysates, we could not detect any truncation of UBB^{+1}. We attribute this to the post-mortem delay since using lysates from mouse brain did yield truncated UBB^{+1}.

AD brains show characteristic features. Intracellular hyperphosphorylated tangles, extracellular amyloid beta plaques as well as UBB^{+1} can be observed in the diseased brains. The origin of these species is essential for understanding the etiology of AD and to see opportunities for a therapeutic strategy. Here, we show that truncated UBB^{+1} cannot be visualized by antibodies used to detect UBB^{+1} in post-mortem tissue. This suggests a new explanation as to why UBB^{+1} is detectable in selective neurodegenerative diseases (Fig. 5). Normally, UBB^{+1} would be truncated by a C-terminal hydrolase (e.g., UCH-L3). Truncation could be impaired in neurodegenerative diseases leading to accumulation of full length UBB^{+1}. According to this hypothesis full length UBB^{+1} could be regarded as a marker for dysfunctional UCH-L3 enzyme. Truncation of UBB^{+1} can be impaired in neurodegenerative disorders due to oxidation of UCH-L3. Further studies need to be performed to determine the exact aberration which results in detectable UBB^{+1} in vivo and its role neurodegenerative disorders.

Acknowledgements

We thank R. van der Schors, Ing. (Free University of Amsterdam, The Netherlands) for providing the mass spectrometry results and Prof. Dr. D.A. Hopkins for correcting the English text. We would also like to thank Drs. R.A.I. de Vos (Laboratory for Pathology, Enschede, The Netherlands), Prof. Dr. R.A.C. Roos and the Netherlands Brain Bank (coordinator Dr. R.I. Huitinga) for providing the tissue from Alzheimer's Parkinson's and Huntington's disease patients with matching control tissue.

This research was supported by the Foundation "De Drie Lichten", the International Foundation for Alzheimer Research (ISAO #06502 and #09514), the International Parkinson Foundation (2008), the Brain Foundation of the Netherlands (#15F07(2).48 and #2008(1).17) and the Van Leersum Foundation KNAW (2008).

Appendix A. Supplementary data

Supplementary data associated with this article can be found, in the online version, at doi:10.1016/j.febslet.2011.06.037.

References

[1] Hershko, A. and Ciechanover, A. (1998) The ubiquitin system. Annu. Rev. Biochem. 67, 425–479.
[2] Nijman, S.M., Luna-Vargas, M.P., Velds, A., Brummelkamp, T.R., Dirac, A.M., Sixma, T.K. and Bernards, R. (2005) A genomic and functional inventory of deubiquitinating enzymes. Cell 123, 773–786.

[3] Samara, N.L., Datta, A.B., Berndsen, C.E., Zhang, X., Yao, T., Cohen, R.E. and Wolberger, C. (2010) Structural insights into the assembly and function of the SAGA deubiquitinating module. Science 328, 1025–1029.
[4] Du, Z. et al. (2010) DNMT1 stability is regulated by proteins coordinating deubiquitination and acetylation-driven ubiquitination. Sci. Signal. 3, ra80.
[5] Wu, X., Yen, L., Irwin, L., Sweeney, C. and Carraway III, K.L. (2004) Stabilization of the E3 ubiquitin ligase Nrdp1 by the deubiquitinating enzyme USP8. Mol. Cell. Biol. 24, 7748–7757.
[6] Larsen, C.N., Krantz, B.A. and Wilkinson, K.D. (1998) Substrate specificity of deubiquitinating enzymes: ubiquitin C-terminal hydrolases. Biochemistry 37, 3358–3368.
[7] Leroy, E. et al. (1998) The ubiquitin pathway in Parkinson's disease. Nature 395, 451–452.
[8] Sultana, R. et al. (2006) Redox proteomics identification of oxidized proteins in Alzheimer's disease hippocampus and cerebellum: an approach to understand pathological and biochemical alterations in AD. Neurobiol. Aging 27, 1564–1576.
[9] Schwartz, A.L. and Ciechanover, A. (2009) Targeting proteins for destruction by the ubiquitin system: implications for human pathobiology. Annu. Rev. Pharmacol. Toxicol. 49, 73–96.
[10] Perry, G., Friedman, R., Shaw, G. and Chau, V. (1987) Ubiquitin is detected in neurofibrillary tangles and senile plaque neurites of Alzheimer disease brains. Proc. Natl. Acad. Sci. USA 84, 3033–3036.
[11] Keck, S., Nitsch, R., Grune, T. and Ullrich, O. (2003) Proteasome inhibition by paired helical filament-tau in brains of patients with Alzheimer's disease. J. Neurochem. 85, 115–122.
[12] Kitada, T. et al. (1998) Mutations in the parkin gene cause autosomal recessive juvenile parkinsonism. Nature 392, 605–608.
[13] Kishino, T., Lalande, M. and Wagstaff, J. (1997) UBE3A/E6-AP mutations cause Angelman syndrome. Nat. Genet. 15, 70–73.
[14] van Leeuwen, F.W. et al. (1998) Frameshift mutants of beta amyloid precursor protein and ubiquitin-B in Alzheimer's and Down patients. Science 279, 242–247.
[15] van Leeuwen, F.W. et al. (2006) Frameshift proteins in autosomal dominant forms of Alzheimer disease and other tauopathies. Neurology 66, S86–S92.
[16] Fischer, D.F. et al. (2003) Disease-specific accumulation of mutant ubiquitin as a marker for proteasomal dysfunction in the brain. FASEB J. 17, 2014–2024.
[17] Lindsten, K., de Vrij, F.M., Verhoef, L.G., Fischer, D.F., van Leeuwen, F.W., Hol, E.M., Masucci, M.G. and Dantuma, N.P. (2002) Mutant ubiquitin found in neurodegenerative disorders is a ubiquitin fusion degradation substrate that blocks proteasomal degradation. J. Cell Biol. 157, 417–427.
[18] Lam, Y.A., Pickart, C.M., Alban, A., Landon, M., Jamieson, C., Ramage, R., Mayer, R.J. and Layfield, R. (2000) Inhibition of the ubiquitin–proteasome system in Alzheimer's disease. Proc. Natl. Acad. Sci. USA 97, 9902–9906.
[19] van Tijn, P., de Vrij, F.M., Schuurman, K.G., Dantuma, N.P., Fischer, D.F., van Leeuwen, F.W. and Hol, E.M. (2007) Dose-dependent inhibition of proteasome activity by a mutant ubiquitin associated with neurodegenerative disease. J. Cell Sci. 120, 1615–1623.
[20] Shabek, N., Herman-Bachinsky, Y. and Ciechanover, A. (2009) Ubiquitin degradation with its substrate, or as a monomer in a ubiquitination-independent mode, provides clues to proteasome regulation. Proc. Natl. Acad. Sci. USA 106, 11907–11912.
[21] Verhoef, L.G., Heinen, C., Selivanova, A., Halff, E.F., Salomons, F.A. and Dantuma, N.P. (2009) Minimal length requirement for proteasomal degradation of ubiquitin-dependent substrates. FASEB J. 23, 123–133.
[22] Lin, M.T. and Beal, M.F. (2006) Mitochondrial dysfunction and oxidative stress in neurodegenerative diseases. Nature 443, 787–795.
[23] Alonso, A. et al. (2002) Inhibition of T cell antigen receptor signaling by VHR-related MKPX (VHX), a new dual specificity phosphatase related to VH1 related (VHR). J. Biol. Chem. 277, 5524–5528.
[24] Gietz, R.D. and Schiestl, R.H. (2007) Microtiter plate transformation using the LiAc/SS carrier DNA/PEG method. Nat. Protoc. 2, 5–8.
[25] Schagger, H. (2006) Tricine–SDS–PAGE. Nat. Protoc. 1, 16–22.
[26] Dantuma, N.P., Lindsten, K., Glas, R., Jellne, M. and Masucci, M.G. (2000) Short-lived green fluorescent proteins for quantifying ubiquitin/proteasome-dependent proteolysis in living cells. Nat. Biotechnol. 18, 538–543.
[27] Shevchenko, A., Wilm, M., Vorm, O. and Mann, M. (1996) Mass spectrometric sequencing of proteins silver-stained polyacrylamide gels. Anal. Chem. 68, 850–858.
[28] Schutz-Geschwender, A., Zhang, Y., Holt, T., McDermitt, D. and Olive, M.D. (2004) Quantitative, Two-Color Western Blot Detection with Infrared Fluorescence. Technical Report, LI-COR Biosciences, Lincoln, NE.
[29] Johnston, S.C., Larsen, C.N., Cook, W.J., Wilkinson, K.D. and Hill, C.P. (1997) Crystal structure of a deubiquitinating enzyme (human UCH-L3) at 1.8 A resolution. EMBO J. 16, 3787–3796.
[30] Johnston, S.C., Riddle, S.M., Cohen, R.E. and Hill, C.P. (1999) Structural basis for the specificity of ubiquitin C-terminal hydrolases. EMBO J. 18, 3877–3887.